Quantitative analysis of susceptibility to intergranular corrosion in alloy 625 joined by friction stir welding

E. B. Fonseca, A. Z. Fatichi, M. Terada, A. F. S. Bugarin, J. Rodriguez, Isolda Costa & A. J. Ramirez

Published online: 02 Dec 2022.

Submit your article to this journal ⍈

Article views: 62

View related articles ⍈

View Crossmark data ⍈

I·M3
Institute of Materials,
Minerals & Mining

Taylor & Francis
Taylor & Francis Group

Check for updates

Quantitative analysis of susceptibility to intergranular corrosion in alloy 625 joined by friction stir welding

E. B. Fonseca [a], A. Z. Fatichi [a], M. Terada [b], A. F. S. Bugarin [b,c], J. Rodriguez [d], Isolda Costa [c] and A. J. Ramirez [e]

aDepartment of Mechanical Engineering, University of Campinas – UNICAMP, Campinas, Brazil; bSENAI Institute of Innovation for Advanced Manufacturing and Microfabrication, São Paulo, Brazil; cIPEN/CNEN-SP, São Paulo, Brazil; dDepartment of Engineering and Basic Science, Universidad EIA, Antioquia, Colombia; eDepartment of Materials Science and Engineering, The Ohio State University, Columbus, OH, USA

ABSTRACT
Alloy 625 is a Ni-based alloy used in aerospace, energy, chemical, oil and gas industries, mainly as cladding material due to its corrosion resistance, high strength and creep resistance at high temperature. In this study, microstructural evaluation and susceptibility to intergranular corrosion of base metal and friction stir welded Alloy 625 were investigated. Friction stir welded joints exhibited a lower corrosion rate and degree of sensitisation compared to the base metal. It is mainly due to grain refinement and lower cooling rate of the friction stir welding process. The stir zone of the present weld has a finer grain structure and lower density of twin boundaries than the base metal and it led to the improvement of the mechanical and corrosion properties.

Introduction

Ni alloys are used in chemical, oil and gas, energy and aerospace industries because they have good resistance to oxidation and corrosion under severe conditions and excellent mechanical properties at elevated temperatures [1,2]. In particular, Alloy 625 is mainly used as a coating material in the oil and gas industry [1,3]. In most of these applications, fusion welding is employed for joining these components. However, when fusion welding is used in nickel alloys, some problems may arise, the major one being hot-cracking in the weld zone due to the segregation of alloying elements during solidification [4]. To alleviate the hot-cracking, careful control of the composition of the weld metal and temperature are usually needed during welding. Even if hot-cracking is suppressed, an as-cast coarse microstructure remains in the fusion zone. Additionally, the heat-affected zone (HAZ) usually undergoes precipitation of Cr-rich carbides and grain growth during fusion welding, which reduces corrosion resistance and ductility respectively [2]. Most of the above-mentioned problems occur in this alloy during fusion welding and are attributed to solidification [5]. Therefore, it would benefit from a solid-state joining process. Friction stir welding (FSW) is an option to effectively avoid the problems caused by fusion welding since it occurs in solid state [1,6–9].

FSW involves a non-consumable rotating tool, composed by a shoulder and a pin, which is inserted into the abutting edges of the sheets or plates to be joined and moves along the joint to be welded [10]. The side of the plate in which the direction of the rotational speed of the tool is the same as the welding direction is called the advancing side, while the other side is called the retreating side [11]. This difference in relative velocities produces asymmetry in heat transfer [12] and material flow on both sides of the weld.

During welding, heating can also promote sensitisation, which is the precipitation of secondary phases, which results in depleted regions of alloying elements important for resistance to localised corrosion. To evaluate in a quantitative manner the sensitivity to intergranular corrosion, the conventional immersion method and electrochemical technique DL-EPR were used. The latter was developed by Cihal [12–14] to characterise the material sensitisation.

Material and methods

The material used in this study was the Alloy 625, provided by Sandmayer Steel Company. The chemical composition of the alloy is described in Table 1.

Welding conditions and process parameters used to produce Alloy 625 joints for further analysis and investigation are presented in Table 2. FSW was performed in 6-mm-thick plates, using a PCBN-WRe tool with a 5.74 mm pin.

Microstructural characterisation

Optical microscopy

Cross-sections of the welded joints were prepared by conventional metallographic procedures and etched in a solution of 10% chromic acid (10 g CrO_3 and 90 mL water), and a voltage of 2.5 V for 20 s.

Electron backscattered diffraction

Electron backscattered diffraction (EBSD) analysis was performed in a scanning electron microscope Thermo Fisher Scientific Quanta 650 FEG to assess the microstructural development after the FSW process. Areas of 100×100 μm^2 were analysed, with a step size of 0.25 μm. Base metal and both welding parameters were analysed.

Table 1. Chemical composition of investigated Alloy 625 (% weight).

Ni	Cr	Mo	Nb	Fe	Si	Ti	Al	Mn	Co	C
60.7	22.5	9.39	3.50	3.00	0.22	0.24	0.18	0.09	0.05	0.02

Table 2. Welding conditions and process parameters.

|	Rotational speed (rev min^{-1})	Welding speed (mm min^{-1})	Axial force (kN)	Heat input (kJ mm^{-1})
1	100	50.8	83.2	4.37
2	75		72.3	3.90

Vickers hardness

Mechanical properties of the welded joints were examined by Vickers microhardness. Hardness maps were obtained across the top of the welded joints using 0.2 kgf load for 15 s.

Double loop electrochemical potentiokinetic reactivation

The susceptibility to intergranular corrosion of the Alloy 625 base metal and welded joints with different values of rotational speed (75 and 100 rev min^{-1}) was quantitatively evaluated by the electrochemical method DL-EPR (Double loop electrochemical potentiokinetic reactivation). DL-EPR tests were performed in an electrochemical cell consisting of three electrodes. A saturated calomel electrode (SCE) and a platinum wire were used as reference electrode and counter electrode, respectively. Alloy 625 specimens acted as the working electrode. Specimens for DL-EPR tests were mounted in epoxy resin and, prior to each electrochemical test, subjected to metallographic preparation up to 1 μm diamond paste (Figure 1).

The electrolyte used consisted of 146 ml of sulphuric acid (H_2SO_4), 120 ml of hydrochloric acid (HCl), 97 mg of potassium thiocyanate (KSCN) and 734 ml of distilled water. All experiments were conducted at 25°C. BioLogic SP-200 potentiostats were used and before each test, the time to stabilise the open circuit potential (OCP) was 120 s. Then, the test was initiated at −100 mV/OCP and the sample was anodically polarised to a potential of +150 mV/SCE at a scanning rate of 6 V h^{-1}. The scanning direction was reversed, and the sample was cathodically polarised, at the same scanning rate, back to the corrosion potential [6]. Thus, two curves were obtained. In the anodic polarisation curve (obtained from −100 mV/OCP to the passivating potential), the current density at the peak is designated as I_a, while the cathodic polarisation curve, which is a reactivation, has the current density peak I_r. Therefore, in this method, the measurement of the degree of sensitisation (DOS) is usually taken as the ratio of the two peak currents I_r/I_a.
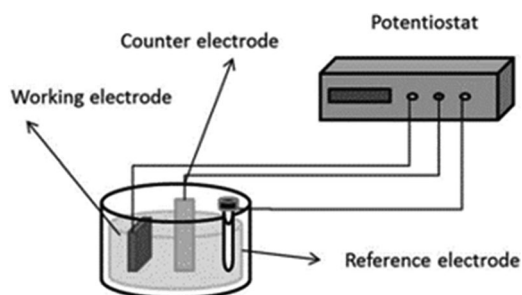
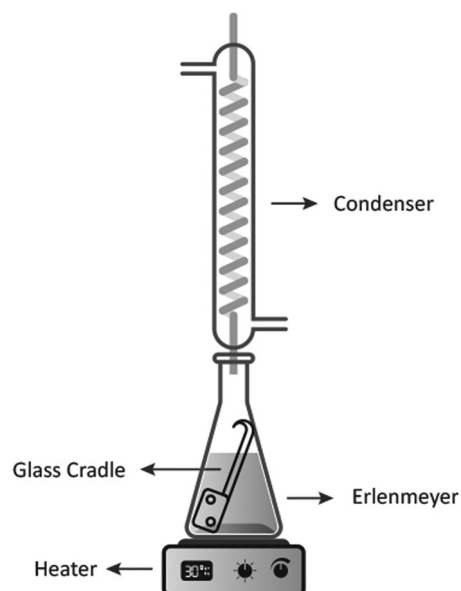## Ferric sulphate-sulphuric acid test

The boiling ferric sulphate-sulphuric acid test (Streicher test) may be applied to Alloy 625 in the welding conditions according to ASTM G28 [15]. This test method is widely used to evaluate the effects of post-weld heat treatments. The total surface area of each specimen subjected to this test method was approximately 20 cm^2 and all the facets of the specimens were ground using 100 grit abrasive SiC paper. Then the samples were degreased using suitable and non-chlorinated agents such as soap and acetone, dried, and weighed with an accuracy of 0.001 g. Subsequently, the samples were inserted into a glass cradle, which guarantees that all surfaces were exposed to the same conditions, as shown in Figure 2.

The specimens were exposed for 120 h to the actively boiling solution consisting of 236 mL of sulphuric acid, 400 mL of distilled water, and 19.75 g of ferric sulphate. At the end of the 120 pre-set hours, the samples were taken out of the solution and carefully cleaned, dried and weighed again to allow the calculation of the total weight changes in order to determine the corrosion rate.

Results

The surface appearance of the joints is shown in Figure 3 [16] and it is observed that, in both cases, good surfaces were obtained with the absence of flash or defects.

Two types of precipitates were found in as-received Alloy 625: MC and $M_{23}C_6$, both with different morphologies. The characterisation of the Alloy 625 base metal was carried out in a previous study [17]. MC precipitates present polygonal shape, with diameters from 5 to 10 μm. MC carbides are Ti and Nb-rich and are preferably located at the grain boundaries. $M_{23}C_6$ are smaller than 1 μm and are rounded or polygonal shaped, located at grain or twin boundaries. $M_{23}C_6$ carbides are enriched in Cr, with some Mo solubility. In

Figure 1. Apparatus for DL-EPR test.

Figure 2. Apparatus for ferric sulphate-sulphuric acid test.
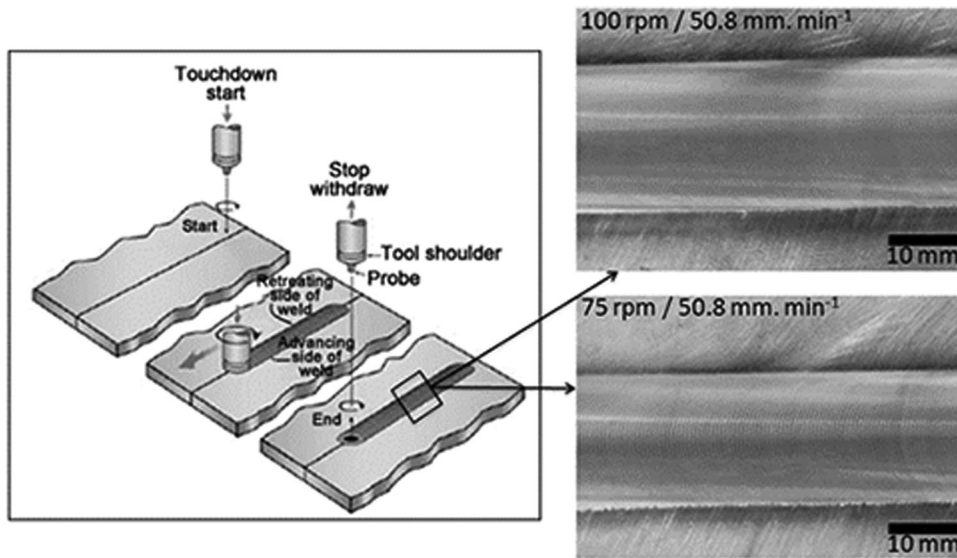
Figure 3. Surface appearance for the Alloy 625 after Friction stir welding.
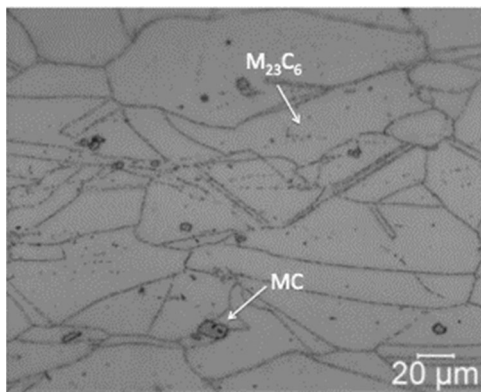
Figure 4. Optical micrographs of Alloy 625: γ matrix with MC and $M_{23}C_6$ carbides.

Figure 4, smaller precipitates can be noticed at grain and twin boundaries. Some bigger carbides are distributed randomly into the grains [16].

The cross-section of the welded joints for both welding parameters showed similar characteristics, as seen in Figure 5.

Figure 5 also shows the microstructural details of the FSWed joints with different rotational speeds, 100 and 75 rev min^{-1}. The microstructural changes between different regions (SZ, TMAZ and BM) can also be observed, exposing a redistribution of precipitates and deformation of the grains, as previously reported in the literature [17]. The MC and $M_{23}C_6$ precipitates identified in the base metal were redistributed according to the material flow and deformation of the grains.

The microstructure of the top surface of FSWed Alloy 625 was investigated by electron backscatter diffraction (EBSD), as shown in Figure 6. Both stir zones presented equiaxed grain structure due to recrystallisation with a significant refinement in grain size as compared to the base metal. The base metal exhibited elongated grain microstructure due to the rolling process, and a grain size of 12.1 ± 1.3 μm.

The stir zones of the two welding conditions, 100 and 75 rev min^{-1}, showed average grain size of 1.06 ± 0.02 and 0.86 ± 0.01 μm, respectively. Vickers hardness maps of the cross-section of the welded joints for the two conditions studied (75 and 100 rev min^{-1} are shown in Figure 7.
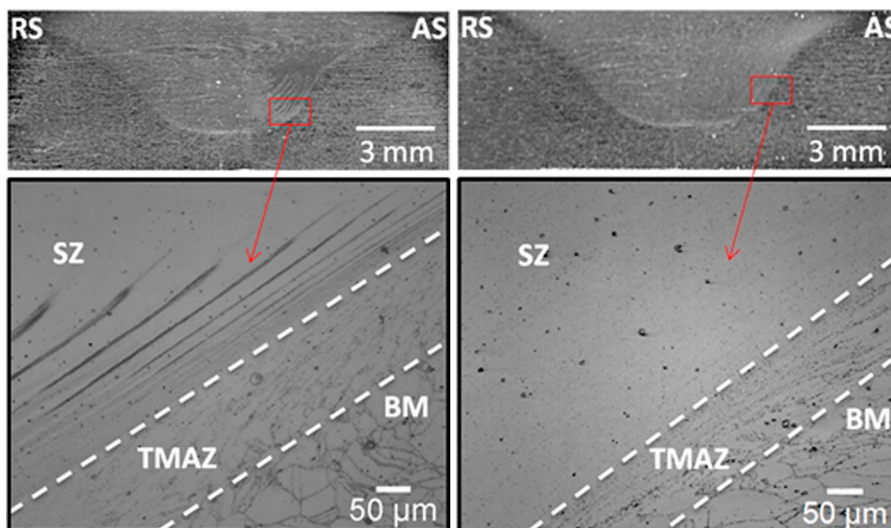
Figure 5. Optical micrographs after electrolytic etching showing the FSW zones.
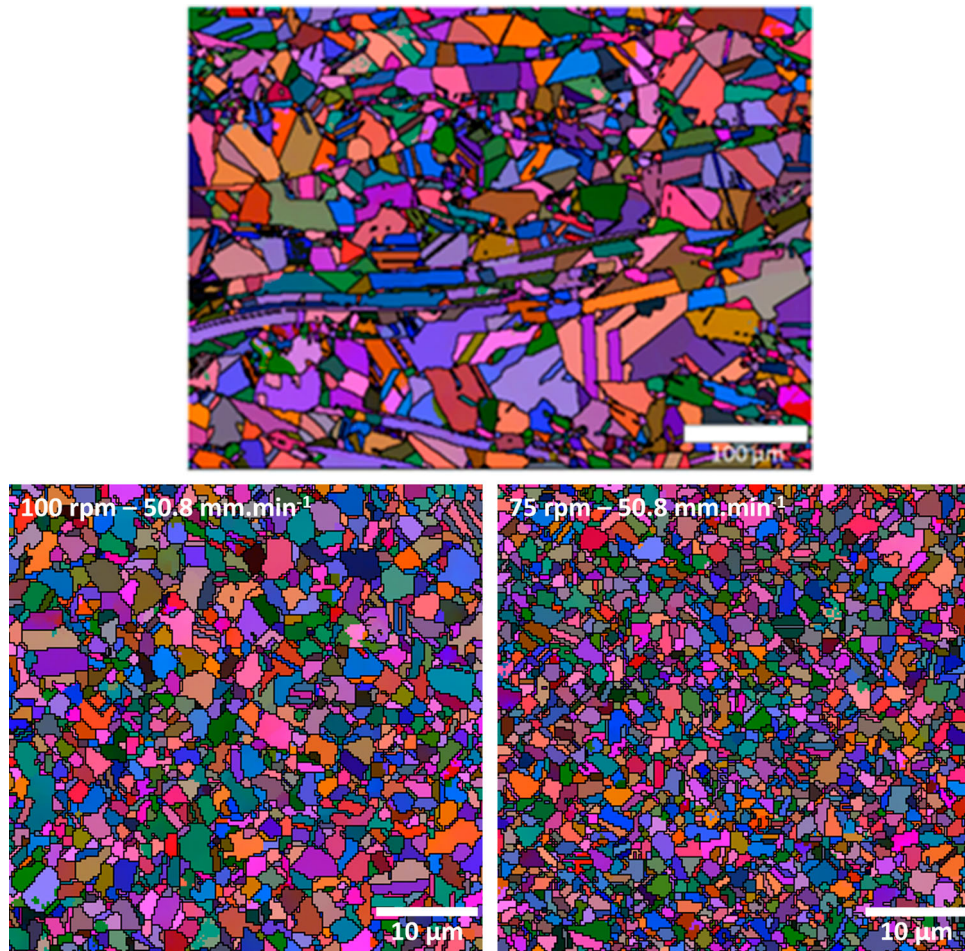
Figure 6. Euler orientation maps obtained for base metal (left) and across the top of the stir zone (centre and right).

The microhardness maps show that the SZ is harder than the BM as a result of the finer microstructure. In addition, the welded joint performed at lower rotational speed presented a finer microstructure, as evidenced by EBSD analysis, thus registered the highest microhardness values, as shown in Table 3.

The results of the DL-EPR test for the base metal and the stir zone are represented in Figure 8 for comparison purposes. SEM images of the alloy 625 after DL-EPR tests are shown in Figure 9(a–c) to base metal, SZ with 75 rev min^{-1} and SZ with 100 rev min^{-1}, respectively. The percentages of the DOS measured by the ratio between the current density

peaks are shown in Figure 10. The SZ of Alloy 625 exhibited a lower DOS (3.53% and 4.52%) compared to the base metal (6.52%), which showed a correlation between higher current densities. Thus, sensitisation resistance of the fine-grained SZ microstructure is higher than that of the BM coarse-grain microstructure.

The corrosion rates obtained by the immersion tests are shown in the histogram of Figure 11. The values were calculated by the following expression:

$$\text{Corrosion Rate} = (K \times W)/(A \times T \times D),$$

where K is a constant (8.76×10^4 for corrosion rate in millimeters per year), T is the time of exposure in hours to the nearest 0.01 h, A is the area in cm^2 to the nearest 0.01 cm^2,
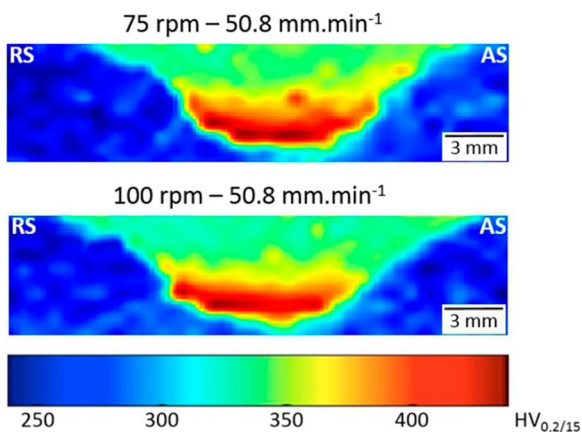
Figure 7. Microhardness maps shows the overall increase of hardness in the welded joint compared to the base metal.
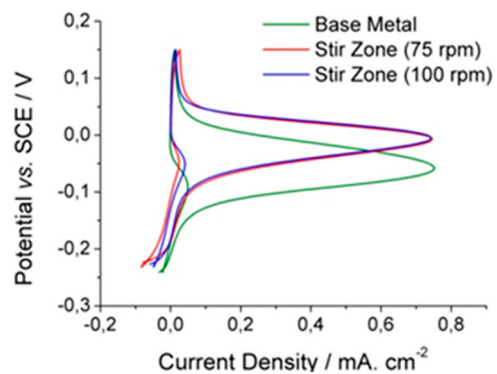
Figure 8. DL-EPR curves for Stir Zone of friction stir welded Alloy 625 and for Base Metal.

Table 3. Highest Vickers microhardness values (HV)

Sample	HV$_{0,2/15}$
Base metal	270 ± 5
Stir zone (75 rev min^{-1})	393 ± 6
Stir zone (100 rev min^{-1})	361 ± 5

W is the mass loss in grams to the nearest 0.001 g and D is the density in g cm^{-3} (8.44 g cm^{-3} for Alloy 625).

The stir zone of friction stir welded joints exhibited a lower corrosion rate (0.38 and 0.42 mm year^{-1}) compared to the base metal (0.49 mm year^{-1}).

Discussion

Intergranular corrosion is typically caused by the precipitation of carbides at grain boundaries. Precipitation consumes Cr, leaving a depleted zone along grain boundaries. Thus, the corrosion rate is affected by the volume fraction of the precipitated carbides per unit area of the grain boundaries. As shown in the time–temperature-transformation diagram of the Alloy 625 [17], carbides form when the material is exposed to temperatures ranging from 800°C and 1000°C for about 1 hour. Liu et al. [18] conducted thermomechanical simulation of the TIG welding HAZ in alloy 617 and concluded that M23C6 carbides were found along grain boundaries in HAZ at lower temperatures (1150°C) and reduced between 1300°C and 1350°C. However, due to the temperature increase from 1150°C to 1350°C the yield and ultimate tensile stresses decrease due to the presence of coarse carbides. In conventional welding, the sensitisation phenomena are significantly delayed in the coarse-grained specimens. This is attributable to the lower driving force available in the coarser microstructures for the diffusion of elements, such as Cr, Mo, and Nb from the grain to the boundary [19,20]. Pulsed current GTAW also produces fine equiaxed dendrites in the fusion zone, and CO_2 laser welding causes micro-level segregation of Cr, Mo, and Ti into interdendritic regions in the fusion zone [21,22]. However, FSW occurs in the solid state and the cooling rate is fast enough to hinder carbide coarsening, forming a shallow Cr depletion zone [2]. It has been reported that FSW of Alloy 625 reaches a peak temperature of 1150°C with a cooling time between 800°C and 500°C ($t_{8/5}$) below 20 s [23]. Therefore, there is not enough time for significant carbide coarsening during FSW. Thus, the area of the grain boundaries has a major influence on sensitisation in this case [24].

Tool wear could also affect the corrosion resistance of the welded joint. It has been reported for steel joints that W and Re might diffuse into the matrix, while boron nitride particles remain as fragments in the SZ [25]. However, according to the literature [8,26], tool wear in FSW of Ni alloys can be reduced when processing at low rotational speeds, such as the ones used in the current study. Binder et al [27] evidence that the increase of boron concentration in Cr–Ni–Co–Fe alloys accelerates the development of complex spinels at the protective oxide Cr_2O_3, improving the corrosion resistance. Vernier et al. [28] found boron atoms – initially in the solid solution in the matrix – incorporated in the protective oxide layer of the Inconel 718. Besides, the literature presents that the addition of B in Ni–Cr superalloys can reduce the agglomeration of M23C6 carbides [29], diminishing the sensitisation. However, in the SEM analyses, no region with an evident concentration of BN particles nor B in solid solution was detected. Thus, the difference in corrosion resistance between the base metal and the welded joint can be attributed to the microstructural refinement and the sensitisation and desensitisation phenomena.
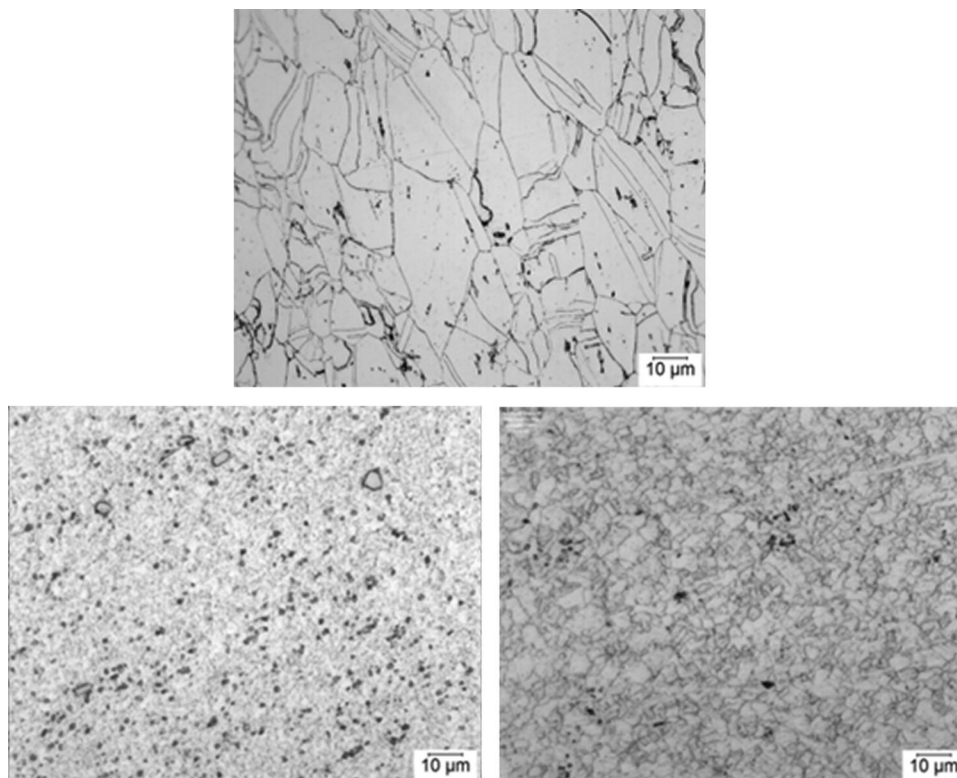
Figure 9. Optical microscopy images of the Alloy 625 after DL-EPR tests (a) base metal, (b) SZ (75 rev min^{-1} and 50.8 mm.min^{-1}) and (c) SZ (100 rev min^{-1} and 50.8 mm min^{-1}).
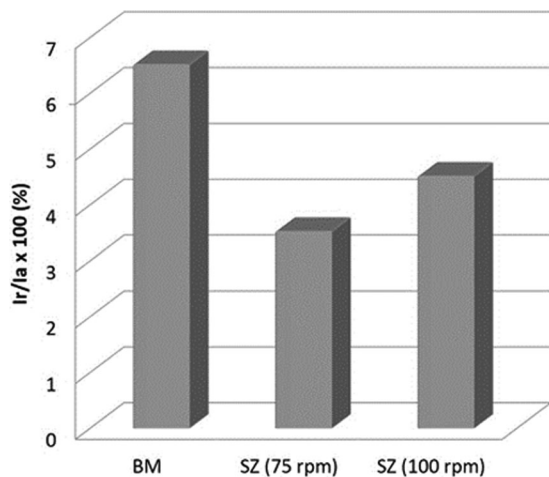
Figure 10. I_r/I_a ratios of the DL-EPR test for the studied conditions of Alloy 625.

Since DL-EPR test is sensitive to Cr depletion, which can be associated with carbide precipitation and/or growth [2], the results can be rationalised as the effectiveness of the sensitisation and desensitisation phenomena. As the grain size decreases, the time required for the desensitisation becomes shorter. Figure 9 presents the difference of the grain size, comparing the base metal (bigger grain size) and the stir zone (smaller grain size). Eventually, the time interval between the sensitisation and desensitisation will be insignificant for sufficiently small grain sizes, because the profusion of grain boundaries allows very efficient diffusion of chromium. In addition, the distances for chromium to diffuse from the grain interior to grain boundaries are very small, so that both factors facilitate the replacement of chromium-depleted regions at the grain boundaries and thus the desensitisation occurs almost simultaneously with sensitisation [30]. This is the main reason for the lower current density ratio (I_r/I_a) of the stir zone in comparison to the base metal, which is shifted towards a lower potential compared to the stir zone, as shown in Figure 10. Thus, the stir zone presents a higher corrosion resistance when compared to the base metal. In contrast, Li et al [31] affirm that the corrosion resistance of Ni-based welded underwater was inferior to that of base metal, but still maintained a high level based on the corrosion current density.
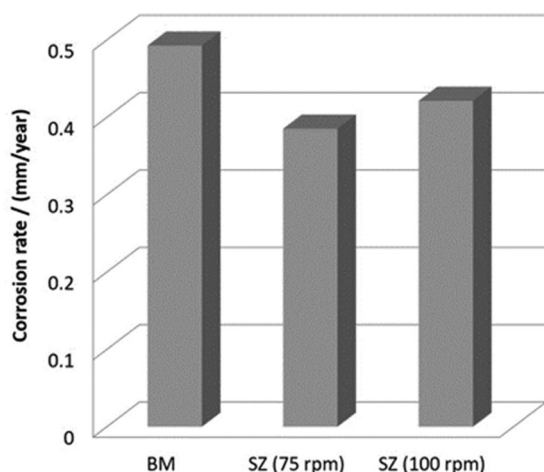
During Streicher test, the corrosion severity is determined by the volume of chromium-depleted zones dissolved, as well as by the volume of detached grains [32]. The results of the DL-EPR tests were similar to those obtained from the Streicher test, showing a good agreement between both tests. The higher the sensitisation of the specimen, the higher the amount of detached grains, and therefore the higher the corrosion rate.

Thus, the DL-EPR analysis is a rapid and reliable method for detecting sensitisation of the Alloy 625 welded by FSW. The test time with this technique is reduced dramatically to a few minutes and it requires smaller samples. Another advantage of this method is its high sensitivity to a lower DOS compared with the standard immersion tests. As a disadvantage, highly skilled laboratory staff is required to execute the DL-EPR tests in a proper way. Another disadvantage of this test is that test parameters must be optimised to each tested material [30].

Conclusions

The welding parameters for Alloy 625 joints showed good results and it was possible to obtain volumetric joints without defects. The application of the FSW process in Alloy 625 leads to a grain refinement of about 20 μm in the base metal to about 1 μm in the stir zone. This resulted in an improvement of mechanical properties of the stir zone, where the hardness increased by about 40% compared to the base metal.

The stir zone of friction stir welded joints exhibited a lower corrosion rate (0.38 and 0.42 mm year^{-1}) compared to the base metal (0.49 mm year^{-1}) according to Streicher test. The stir zone exhibited a lower DOS (3.53% and 4.52%) compared to the base metal (6.52%) according to DL-EPR test, due mainly to grain refinement, which reduces the time required for desensitisation. Both tests exhibited similar results, so there is a good agreement between Streicher and EPR tests in the investigated conditions.

Disclosure statement

No potential conflict of interest was reported by the author(s).

Funding

Figure 11. Corrosion rates calculated for the studied conditions of Alloy 625 by the ferric sulphate-sulphuric acid test.

ORCID

E. B. Fonseca http://orcid.org/0000-0002-6437-6125
A. Z. Fatichi http://orcid.org/0000-0003-2235-3774
M. Terada http://orcid.org/0000-0002-2011-5759
A. F. S. Bugarin http://orcid.org/0000-0002-0386-8142
J. Rodriguez http://orcid.org/0000-0003-3219-6290
Isolda Costa http://orcid.org/0000-0002-4987-3334
A. J. Ramirez http://orcid.org/0000-0002-4252-2857

References

[1] Lemos GVB, Farina AB, Piaggio H, et al. Mitigating the susceptibility to intergranular corrosion of alloy 625 by friction-stir welding. Sci Rep. 2022;12(1):3482.

[2] Sato YS, Arkom P, Kokawa H, et al. Effect of microstructure on properties of friction stir welded Inconel Alloy 600. Mater Sci Eng A. 2008;477(1–2):250–258.

[3] Lackner R, Mori G, Egger R, et al. Sensitization of as rolled and stable annealed alloy 625. BHM Berg- Huettenmaenn Monatsh. 2014;159(1):12.

[4] Winowlin Jappes JT, Ajithram A, Adamkhan M, et al. Welding on Ni based super alloys – a review. Mater Today: Proc. 2022;60:1656–1659.

[5] Song KH, Nakata K. Effect of precipitation on post-heat-treated Inconel 625 alloy after friction stir welding. Mater Des. 2010;31 (6):2942–2947.

[6] Fernandez JR, Ramirez AJ. Microstructural evolution during friction stir welding of mild steel and Ni-based alloy 625. Metall Mater Trans A. 2017;48(3):1092–1102.

[7] Aonuma M, Iwaoka T, Nakamura I, et al. Dissimilar Lap joining of commercial pure titanium to nickel-based alloy by friction stir welding. Q J Jpn Weld Soc. 2017;35(2):85s–88s.

[8] Lemos GVB, Farina AB, Nunes RM, et al. Residual stress characterization in friction stir welds of alloy 625. J Mater Res Technol. 2019;8(3):2528–2537.

[9] Mishra RS, Ma ZY. Friction stir welding and processing. Mater Sci Eng: R: Rep. 2005;50(1–2):1–78.

[10] Nandan R, DebRoy T, Bhadeshia HKDH. Recent advances in friction-stir welding – Process, weldment structure and properties. Prog Mater Sci. 2008;53:980–1023.

[11] Cho JH, Boyce DE, Dawson PR. Modeling strain hardening and texture evolution in friction stir welding of stainless steel. Mater Sci Eng A. 2005;398(1–2):146–163.

[12] Číhal V, Štefec R, Shoji T, et al. Electrochemical potentiodynamic reactivation: development and applications of the EPR test. Key Eng Mater. 2004;855:261–263.

[13] Cihal V. No intergranular corrosion of steels and alloys. Campinas: (Elsevier B.V; 1984).

[14] Číhal V, Štefec R. On the development of the electrochemical potentiokinetic method. Electrochim Acta. 2001;46(24–25):3867–3877.

[15] ASTM International. (2008).

[16] Threadgill PL, Leonard AJ, Shercliff HR, et al. Friction stir welding of aluminium alloys. Int Mater Rev. 2009;54(2):49–93.

[17] Rodriguez J, Ramirez AJ. Microstructural characterisation of friction stir welding joints of mild steel to Ni-based alloy 625. Mater Charact. 2015;110:126–135.

[18] Liu W, Lu F, Yang R, et al. Gleeble simulation of the HAZ in Inconel 617 welding. J Mater Process Technol. 2015;225:221–228.

[19] Kaithwas CK, Bhuyan P, Pradhan SK, et al. 'Hall-Petch' type of relationship between the extent of intergranular corrosion and grain size in a Ni-based superalloy. Corros Sci. 2020;175:108868.

[20] Xu L, Shao C, Tian L, et al. Intergranular corrosion behavior of Inconel 625 deposited by CMT/GTAW. Corros Sci. 2022;201.

[21] Farahani E, Shamanian M, Ashrafizadeh F. A comparative study on direct and pulsed current gas tungsten arc welding of alloy 617. AMAE Int J ManufMaterl Sc. 2012;2 :1–6.

[22] Ren W, Lu F, Yang R, et al. A comparative study on fiber laser and CO_2 laser welding of Inconel 617. Mater Des. 2015;76:207–214.

[23] Rule JR, Lippold JC. Physical simulation of friction stir welding and processing of nickel-base alloys using Hot torsion. Metall Mater Trans A. 2013;44(8):3649–3663.

[24] Lackner R, Mori G, Prohaska M, et al. (2013).

[25] Giorjão RAR, Pereira VF, Terada M, et al. Microstructure and mechanical properties of friction stir welded 8 mm pipe SAF 2507 super duplex stainless steel. J Mater Res Technol. 2018.

[26] Hanke S, Lemos GVB, Bergmann L, et al. Degradation mechanisms of pcBN tool material during Friction Stir Welding of Ni-base alloy 625. Wear. 2017;376-377:403–408.

[27] binder1953. (n.d.)

[28] Vernier S, Andrieu E, Laffont L. Flash oxidation tests to evidence the segregation of boron at the grain boundaries of superalloy Inconel 718. Materialia (Oxf). 2021;15.

[29] Yang F, Hou J, Gao S, et al. The effects of boron addition on the microstructure stability and mechanical properties of a Ni-Cr based superalloy. Mater Sci Eng A. 2018;715:126–136.

[30] Lakshminarayanan AK, Balasubramanian V. Sensitization resistance of friction stir welded AISI 409 M grade ferritic stainless steel joints. Int J Ad Manuf Technol. 2012;59(9):961–967.

[31] Li H, Liu S, Sun F, et al. Preliminary investigation on underwater wet welding of Inconel 625 alloy: microstructure, mechanical properties and corrosion resistance. J Mater Res Technol. 2022;20:2394–2407.

[32] Prohaska M, Kanduth H, Mori G, et al. On the substitution of conventional corrosion tests by an electrochemical potentiokinetic reactivation test. Corros Sci. 2010;52(5):1582–1592.